JOURNAL OF MATERIALS SCIENCE **33** (1998) 4893–4903

Processing and creep resistance of nickel/yttria composites

LIAN-CHAO SUN, L. L. SHAW
Department of Metallurgy and Materials Engineering, University of Connecticut, Storrs, CT 06269-3136, USA
E-mail: lshaw@mail.ims.uconn.edu

In this study, pure nickel and yttria (Y_2O_3) were selected as a model system to investigate the feasibility of processing metal matrix composites (MMCs) through a powder metallurgy approach for the *in-situ* formation of a continuous three-dimensional reinforcement network or the *in-situ* formation of discrete reinforcements with certain degrees of interconnected clusters. Composites with a volume fraction of Y_2O_3 ranging from 20 to 50% were prepared through hot pressing. The density, microstructure and creep resistance of these composites were evaluated as a function of the yttria volume fraction. It was found that a continuous Y_2O_3 network was formed in composites with 40 and 50 vol % Y_2O_3, while yttria was discrete with some degrees of interconnected clusters in composites with 20 and 30 vol % Y_2O_3. The creep rate was reduced by two to three orders of magnitude with the addition of 20 to 30 vol % Y_2O_3, and it continued to decrease with increasing the volume fraction of yttria to 50%. The analysis indicated that the load transfer to isolated yttria particles could not account for the improved creep resistance of composites with 20 and 30 vol % Y_2O_3, while the load transfer to a continuous yttria network in composites with 40 and 50 vol % Y_2O_3 could not be approximated by the model of the load transfer to continuous fibres. The discrepancies are believed to be related to the presence of interconnected yttria clusters, the low relative density of the yttria phase in the composite, and the low load-carrying capability through a three-dimensional network in comparison with the load-carrying capability through continuous fibres. It is suggested that the density of the yttria phase and hence the creep resistance of the composite can be further improved over what have been obtained in this study by densifying the composite at high temperatures and pressures.

1. Introduction

The materials used at high-temperature environment must possess high strength, high creep resistance and high oxidation resistance. Because the nickel-based alloys have a face centred cubic (f.c.c) structure that is able to maintain good tensile, rupture and creep resistance properties to a much higher temperature than body centred cubic (b.c.c) systems, they have been widely used at high temperature environments. In the past 40 years, many methods have been adopted to strengthen high-temperature alloys, such as solid solution strengthening, precipitation strengthening and dispersion strengthening [1]. Therefore, nickel alloys were developed from the simple nickel–chromium matrix to the multi-elements, multi-phase systems. It is well recognized that the most effective way to maintain strength at temperatures above which γ' goes into solution is to employ a different, stable, non-metallic dispersoid phase. These phases must have chemical, crystallographic and microstructural stabilities at high temperatures. Thus, the dispersoid is required to have a high melting point, high modulus, low solubility and low diffusion rates in the matrix. For high-temperature service, the best dispersoid materials are oxides having high free energies of formation, such as thoria, yttria and lanthana. In addition, it is well known that the size and distribution of the dispersoid phase govern its effectiveness as a strengthener. The particles must be small and uniformly distributed, and for the best balance of the strength and ductility about 2 vol % of dispersoid with a particle size of 10–100 nm and interparticle spacing of 100–500 nm has been proved to be optimum [2]. Based on these understandings, a series of oxide dispersion-strengthened (ODS) Ni-based superalloys have been developed. Nevertheless, the nickel-based superalloys have been utilized up to the 80% of their melting points. Therefore, there is little chance of any dramatic improvements in their operation temperatures only relying on the conventional solid solution-, precipitation- and dispersion-strengthening methods [1].

With the development of the composite science and technology, it is possible to develop new high temperature materials based on composite approaches. A substantial amount of research on metal–matrix

composites (MMCs) has shown that unidirectional fibre composites exhibit superior specific strength and creep resistance along their fibre axis [3, 4]. However, their transverse properties are normally lower–in some cases significantly lower–than those from the corresponding unreinforced matrices [5–9]. Clearly, more balanced transverse properties are required for widespread applications of MMCs. One obvious approach to obtain composites with balanced transverse properties is to develop three-dimensionally reinforced composites. Moreover, for the best creep resistance the reinforcement should be continuous in three dimensions, that is, a three-dimensional self-interconnected reinforcement network is expected to provide the best balanced creep resistance. In addition, from processing and cost-effective viewpoints, it is highly desired that the reinforcement can be formed *in situ* during the fabrication of composites. As such, in this study the feasibility of processing nickel-based composites through a powder metallurgy approach for the *in-situ* formation of a continuous three-dimensional reinforcement network or the *in-situ* formation of discrete reinforcements with certain degrees of interconnected clusters was explored. As the first attempt, pure nickel and yttrium oxide were selected as a model system in this study. The connectivity of the reinforcement (i.e. yttria in this study) as a function of its volume fraction and the microstructural dependency of the creep resistance of these model composites were investigated.

2. Experimental procedure

2.1. Fabrication of composites

Both the yttria and nickel powder, shown in Fig. 1, were supplied by Johnson Matthey Co. and had a purity of 99.9%. The particle size of the nickel powder ranged from 2 to 7 μm and that of the yttria powder from 0.4 to 5 μm. Both nickel and yttria were solid particles without internal voids. Composites with 20, 30, 40 and 50 vol % of yttria were prepared by mixing nickel and yttria powders in the desired volume fraction through dry milling with zirconia balls for 10 h. Uniform mixing was not pursued because of the intention of this study to prepare a continuous three-dimensional reinforcement network or discrete reinforcements with certain degrees of interconnected clusters. The dry mixing described above proved to be an adequate method to achieve this goal (see the Results section for details). The mixed powder was first cold pressed at 30 MPa in a graphite die with a graphite foil as a liner, and then hot pressed at a temperature of 1250 °C with a pressure of 40 MPa for 1 h under a vacuum of less than 1.33×10^{-3} Pa. To obtain the baseline properties, pure nickel and pure yttria samples were also fabricated under the same conditions as the composites. In addition, a pure yttria sample was also hot pressed at 1500 °C to examine the effect of temperature on the density of pure yttria.

2.2. Creep testing

The creep resistance of the composites were evaluated using a compressive test setup since compression testing can utilize small specimens. The creep specimens had a rectangular bar geometry with a height of 10 mm and a cross-section of 5.08×3.81 mm. To minimize the effect of friction, BN spray was applied on both the top and bottom faces of specimens. The test was conducted using a servo-hydraulic machine in vacuum (1.33×10^{-2} Pa) under a load-controlled condition at 1000 °C with a nominal stress of either 20 MPa or 40 MPa. A uniform heating zone of 60 mm height within the vacuum chamber was provided by tantalum resistance foils. The temperature of the specimen during tests was measured by a thermocouple touching directly to the specimen. No extensometer was employed. Instead, the crosshead displacement was recorded and used to compute the creep strain of specimens. The setup could resolve strains of 0.0002% for the specimens used. The estimation of the deformation from the loading train indicated that the contribution from the loading train did not excess 1% of the total strain measured. The linear ordinary least squares method was utilized to analyze creep data. Specifically, to calculate the creep rate, $\dot{\varepsilon}$, at any time t, the creep strain at that point and the creep strains and times at three previous and three following points were used. The equation used is [10]

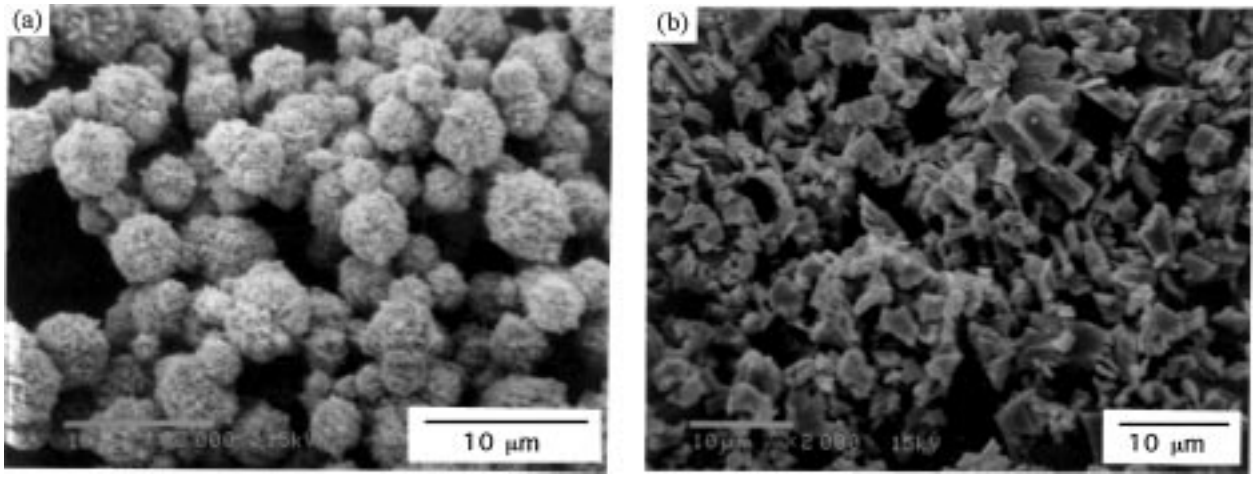

Figure 1 SEM images of (a) nickel and (b) yttria powders used in this study.

$$\dot{\varepsilon} = \frac{7\sum_{i=1}^{7}\varepsilon_i t_i - \sum_{i=1}^{7}\varepsilon_i \sum_{i=1}^{7} t_i}{7\sum_{i=1}^{7} t_i^2 - \sum_{i=1}^{7} t_i \sum_{i=1}^{7} t_i} \quad (1)$$

2.3. Microstructural and other characterizations

The microstructure of pure nickel, yttria and composites was examined in a high-resolution environmental scanning electronic microscope (Phillips ESEM 2020). The connectivity of the yttria phase in the composite specimens was evaluated by etching away the nickel matrix using a dilute nitric acid, followed by comparing the remaining yttria on the top layer of the etched specimen with the average volume fraction of the specimen. The density of the specimens was measured based on the Archimedes' principle.

3. Results

3.1. Microstructure and density of nickel/yttria composites

Microstructures of pure nickel and their composites are shown in Fig. 2. It can be seen that under the

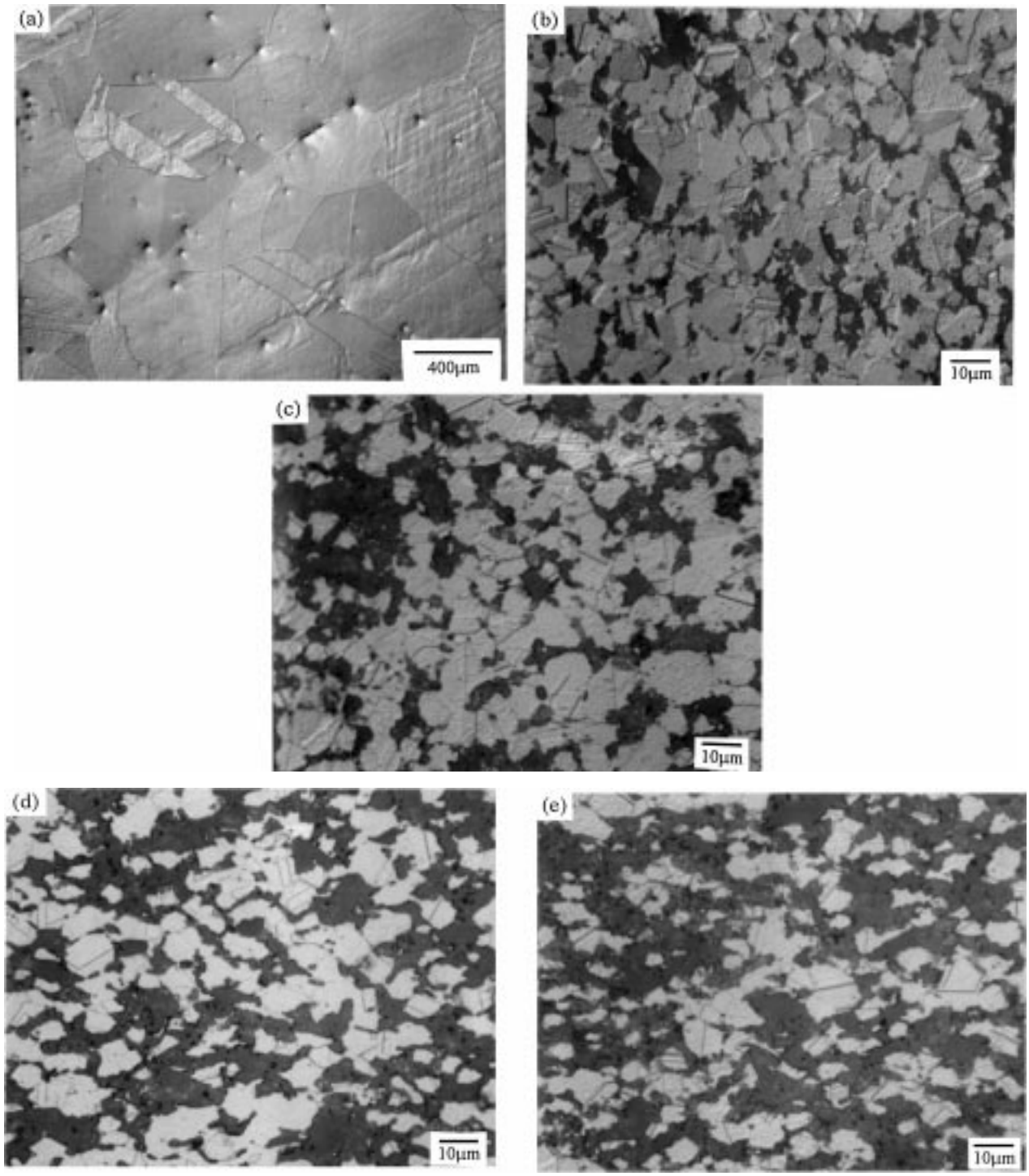

Figure 2 Typical microstructures of (a) hot-pressed pure nickel, and (b), (c), (d) and (e) hot pressed composites with 20, 30, 40 and 50 vol % Y_2O_3, respectively.

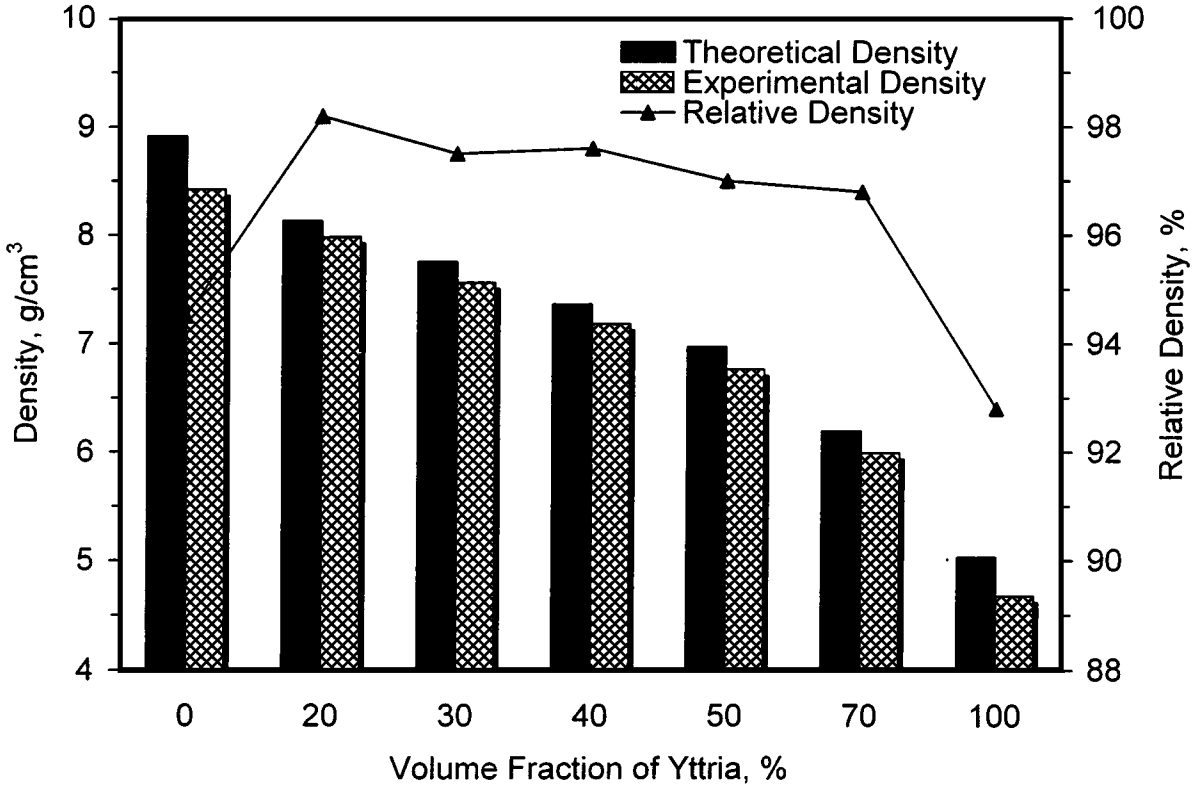

Figure 3 Densities of hot-pressed nickel, yttria and their composites.

present hot pressing condition, grain growth has occurred in pure nickel and the average grain size has reached 1000 μm in diameter at the hot-pressed condition. Furthermore, pores are present within grains and along grain boundaries. Because of the presence of an appreciable amount of pores, the corresponding density of pure nickel is only about 93% of its theoretical (Fig. 3). However, it is noted that the grain growth of nickel and pores within the nickel phase are effectively eliminated and the relative density of the material is increased with the addition of yttria, as shown in Figs 2 and 3. Furthermore, It can be seen from Fig. 2 that yttria with a certain degree of interconnected clusters has formed in all the composites prepared, as we desired originally.

Even with the grain growth inhibition and pore-elimination of the nickel phase by the addition of yttria, it is found that densities of the composites are still lower than those calculated according to the rule of mixtures, as shown in Fig. 3. Closer examination of the microstructure of all the composites (Fig. 2) indicates that nickel phase is 100% dense, while there are pores in the yttria phase. Thus, the fact that the densities of the composites are lower than the theoretical calculation is attributed to the presence of pores in the yttria phase.

Estimation of the yttria grain size at the as-hot pressed condition is conducted using the fracture surface of pure yttria fractured at room temperature (Fig. 4). As can be seen from Fig. 4, the grain size and morphology of pure yttria hot pressed at both 1250 and 1500 °C can be easily identified from their fracture surfaces. It is clear that little grain growth has occurred for pure yttria hot pressed at 1250 °C, while grain growth has taken place for yttria hot pressed at 1500 °C. The relative density measured using the Archimedes' principle is 92.5 and 96.8% for yttria hot pressed at 1250 and 1500 °C, respectively. Pores can also be easily identified from the fracture surface of specimens hot pressed at 1250 °C, as shown by arrows in Fig. 4. These results indicate that the hot pressing temperature of 1250 °C is not high enough to obtain fully dense pure yttria, and confirm that the low relative density of the composites is related to the insufficient densification of the yttria phase in the composites.

The typical microstructures of composites with 20 and 40 vol % Y_2O_3 etched deeply with a dilute nitric acid are shown in Fig. 5. With this etchant the nickel phase is etched away, while the yttria phase is intact. Thus, most of the pores and holes in Fig. 5 can be considered to be the location of the nickel phase before etching. It seems that a continuous Y_2O_3 network has formed in composites with 40 vol % of Y_2O_3. Examination of composites with 20 vol % of Y_2O_3 suggests that a certain degree of connectivity among the Y_2O_3 phase itself has been obtained as some Y_2O_3 phases stand out of the plane of the etched nickel phase. However, the Y_2O_3 phase has not formed a continuous network yet. Thus, the microstructure of composites with 20 vol % Y_2O_3 can be described as possessing discrete Y_2O_3 particles with some degrees of connectivity between these particles. Examination of composites with 30 and 50 vol % Y_2O_3 indicates that composites with 30 vol % Y_2O_3 have a similar microstructure as composites with 20 vol % Y_2O_3, while composites with 50 vol % Y_2O_3 have a similar microstructure as composites with 40 vol % Y_2O_3.

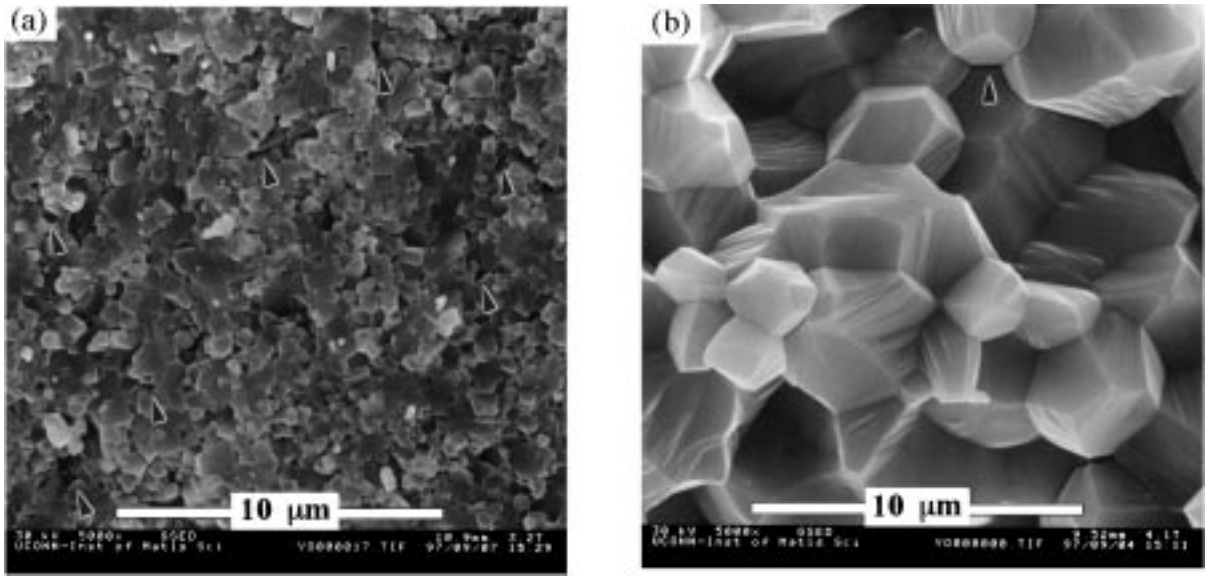

Figure 4 Fracture surfaces of yttria hot pressed at (a) 1250 °C and (b) 1500 °C.

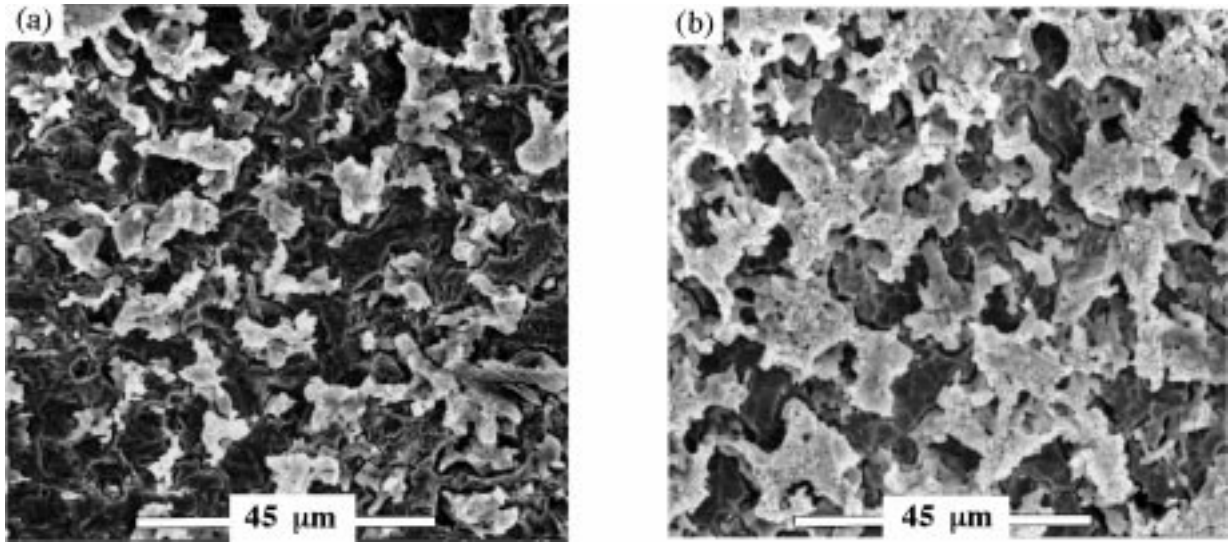

Figure 5 Microstructures of composites with (a) 20 and (b) 40 vol % Y_2O_3 deeply etched with a dilute nitric acid.

3.2. Creep behaviour and resistance

The creep strain of pure nickel versus time is shown in Fig. 6 where the test is stopped before the failure of the specimen. As shown in the figure, the creep of pure nickel exhibits: (i) an instantaneous strain; (ii) a normal primary stage, where the creep rate decreases continuously with time; and (iii) a secondary stage (i.e. steady-state stage), where the creep rate is approximately constant. It can be seen that under the current temperature and loading conditions (1000 °C and 20 MPa) a large compressive creep strain has occurred (∼ 80%) and no true steady-state stage is achieved due to the continuously increased cross section of the creep specimen.

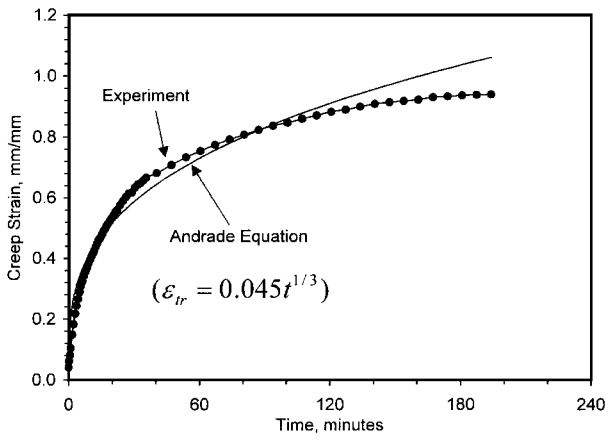

Figure 6 A typical creep strain–time curve of pure nickel under a stress of 20 MPa and at 1000 °C, superimposed with a creep curve calculated using the Andrade equation.

The creep curves of composites with 20 vol % Y_2O_3 under different nominal stresses are shown in Fig. 7. The tests are again stopped before the failure of the specimens. It can be seen that the composites exhibit a similar creep behaviour as the pure nickel, i.e. an instantaneous strain, a normal primary stage and a steady-state stage. Note that the creep strain has been reduced dramatically from ∼ 80% for pure nickel to ∼ 1% for the composite if the creep strains of pure nickel and the composite with 20 vol % Y_2O_3 under a nominal compressive stress of 20 MPa at 100 min are compared. Composites with 30 vol % Y_2O_3 exhibit a similar creep behaviour as composites with 20 vol % Y_2O_3. However,

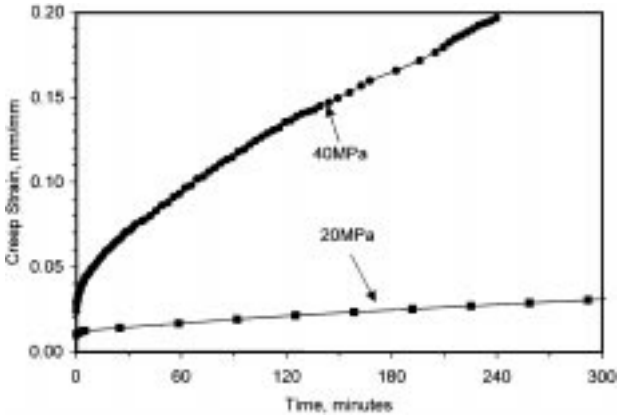

Figure 7 Typical creep curves of composites with 20 vol % Y_2O_3 at 1000 °C under a stress of 20 and 40 MPa.

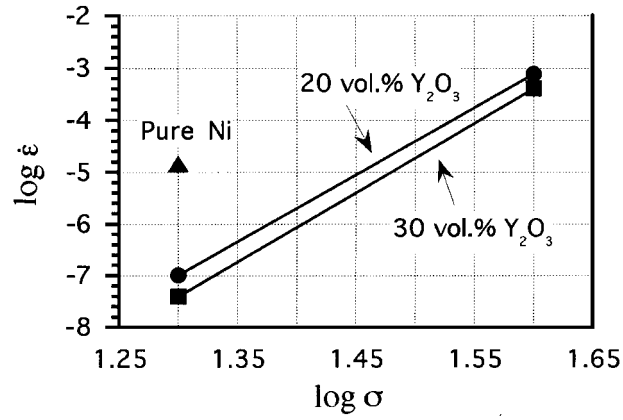

Figure 9 The dependency of the steady state creep rate of the composite on the applied stress.

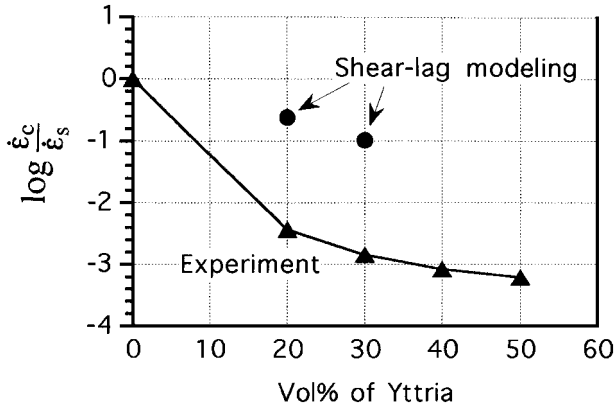

Figure 8 The plot of the steady state creep rate of the composite, $\dot{\varepsilon}_c$, normalized by the steady-state creep rate of the matrix, $\dot{\varepsilon}_s$, versus the volume fraction of yttria.

composites with 40 and 50 vol % Y_2O_3 do not display a minimum creep rate; instead, they exhibit a continuously decreased creep rate up to the time of 5 h at which time the test is stopped. In order to compare the creep rates between various composites and pure nickel, the average creep rate between 100 and 200 min is taken to be characteristic creep rate for each material and a plot of the creep rate normalized by the creep rate of pure nickel versus the volume fraction of Y_2O_3 is presented in Fig. 8. Note that the average creep rate between 100 and 200 min is the steady-state creep rate for composites with 20 and 30 vol % Y_2O_3 and approximately for pure nickel (to be discussed more in Section 4.2). It can be seen from Fig. 8 that the creep rate of composites decreases with the increase of the yttria volume fraction.

The effect of the applied stress on the steady state creep rate is presented in Fig. 9, where a logarithmic scale is used for both the steady-state creep rate and the applied stress. The stress exponent, *n*, calculated from the slope of the curve was 12.9 and 13.4 for composites with 20 and 30 vol % Y_2O_3, respectively.

4. Discussion

4.1. Microstructure and density of nickel/yttria composites

The presence of pores in pure nickel and the corresponding low relative density as shown in Figs 2 and 3 are caused by the hot-pressing condition that is within the time–temperature regime for pores to separate from grain boundaries. It is well known that the pore–grain boundary separation happens when strong grain growth occurs due to a sintering temperature that is too high before a high density has been achieved [11]. The pore–grain boundary separation always leads to a sintered body with a low relative density due to the slow diffusion through the lattice. Thus, a sintering temperature lower than 1250 °C should be used to densify pure nickel powders used in this study.

With the addition of Y_2O_3, the grain growth of the nickel phase is substantially reduced, suggesting that yttria is a good grain growth inhibitor for nickel. Accompanied with the inhibition of the grain growth, the nickel phase in the composites is densified to the full density. However, the densities of these composites are still lower than those calculated according to the rule of mixture. A close examination of Fig. 3 indicates that the highest relative density, 98.2%, is achieved in composites with 20 vol % Y_2O_3, and the relative density of composites decreases with increasing the volume fraction of yttria. These data suggest that the low relative density of the composite is due to the insufficient densification of the yttria phase. This is confirmed by the presence of pores in the yttria phases in the composite, as revealed in Fig. 2. The observed low relative density of the yttria phase both in the composites and in the pure form hot pressed at 1250 °C is consistent with works by other investigators [12, 13]. It is reported that a relative density of 65% of pure yttria results when the free sintering temperature is between 1450 and 1600 °C [12]. However, the relative density increases to 98.6% when the sintering temperature is increased to 1800 °C [13]. Also, a dramatic density increase can be achieved by increasing the applied pressure during densification. For example, a relative density of 99.6% is achieved with the use of hot isostatic pressing at 1250 °C under a pressure of 150 MPa for 45 min [13]. Thus, it is clear that the further increase in the densification of the yttria phase can be achieved by either increasing the hot pressing temperature and/or pressure.

The selection of 1250 °C as the hot-pressing temperature for the present composite is based on the consideration of the melting point of the nickel phase

(1455 °C). Note that the hot-pressing temperature of 1250 °C is 88% of the melting point of nickel in the absolute temperature scale. However, the present results suggest that nickel/yttria composites can be densified at temperatures higher than 88% of the melting point of nickel without the risk of the grain growth and pore-grain boundary separation. This is important from the viewpoint of composite fabrication because high hot-pressing temperatures increase the relative density of the yttria phase and, hence, the relative density of the composite. Thus, based on these results, it can be concluded that it is possible to obtain nickel/yttria composites with a full density by hot pressing the nickel/yttria composites at a temperature higher than 1250 °C and/or with an applied pressure higher than 40 MPa.

4.2. Creep behaviour of pure nickel

The creep data of pure nickel measured in this study are consistent with those reported by other investigators in two aspects: (i) the transient creep strain in the primary stage (ε_{tr}) can be described by Andrade equation [14–16]

$$\varepsilon_{tr} = \beta t^{1/3} \tag{2}$$

where t is the time and β is a constant for the given temperature and stress. Using the curve fitting approach, β was found to be 0.045 for testing conditions of 1000 °C and 20 MPa (see Fig. 6); and (ii) the creep rate at the time of 100 min equals to the steady state creep rate, $\dot{\varepsilon}_s$, of pure nickel calculated from the following phenomenological equation [17, 18]

$$\dot{\varepsilon}_s = B\left(\frac{G}{T}\right)\left(\frac{\sigma}{G}\right)^{4.6} \exp\left(-\frac{Q}{RT}\right) \tag{3}$$

where Q is the apparent creep activation energy and equals 278.4 kJ mol^{-1}, B is a coefficient having a value of 1.31×10^{15} deg s^{-1} Pa^{-1}, R and T have their usual meanings, and G is the shear modulus of nickel and its temperature dependency is described by [19]

$$G = 9.2 \times 10^{10} - 3.37 \times 10^{7}\ T\ (\text{Pa}) \tag{4}$$

Recall that no true steady-state stage is achieved in this study because of the continuously increased cross-section of the specimen during the compressive test. However, it is noted from Fig. 6 that beyond about 85 min, the change of the creep rate becomes small, suggesting that the steady-state creep starts at about 85 min if a constant stress were applied. Thus, Equation 3 will be utilized in this study to compute the steady-state creep rate of the nickel phase in the composite.

4.3. Creep behaviour of composites

The experimental data in this study show that the creep rate of the composite is at least two orders of magnitude lower than that of the nickel matrix. Furthermore, the stress exponent ($n = 13$) of composites with 20 and 30 vol % Y_2O_3 is found to be higher than that ($n = 4.6$) of the matrix. These findings for the nickel/yttria composite are similar to those for aluminium matrix composites reinforced with particulates or whiskers that normally exhibit high values of both the stress exponent and activation energy [20–25]. Several attempts have been made to explain the improved creep resistance and high values of the stress exponent and activation energy of aluminum matrix composites. These include: (i) the concept of the threshold stress [21–25]; (ii) the shear–lag approach [26–29]; (iii) load transfer to isolated short fibres or an interconnected fibre network using finite element analysis [30, 31]; (iv) increased dislocation density around the reinforcement [32–34]; and (v) residual stresses arising from the difference in coefficients of thermal expansion between the matrix and reinforcement [35]. Some questions regarding these proposed mechanisms have been raised. For example, it is unclear how the last two mechanisms above would cause a change in the stress exponent for creep of the composite material [31]. The need to use the non-continuum mechanics approach via the threshold stress concept is troubling because of the coarse scale of the reinforcement. Furthermore, the threshold stress predicted according to various strengthening processes is normally lower than that required for the improved creep resistance [25]. The shear–lag approach with bonded interfaces and the load transfer to isolated reinforcements using finite element analysis only result in a creep law for the composite that has the same stress and temperature dependence as that for the matrix [27, 31]. However, the load transfer to an interconnected reinforcement network does offer a good description of the creep behaviour of aluminium matrix composites [31]. Despite of the aforementioned shortcomings, the threshold stress concept and the shear–lag modelling will be utilized to compare with the observed creep behavior of nickel/yttria composites. This is because that the threshold stress concept provides a reasonable explanation for high values of the stress exponent and activation energy [21–25], while the continuum mechanics approach using shear–lag modelling is consistent with the scale of the reinforcement (note that the size of yttria clusters ranges from 5 to 30 μm, Fig. 2).

Various origins of the threshold stress have been suggested [21–25, 36–39]. Among them, the concepts of the detachment stress for a dislocation to escape from the attractive dislocation–particle interaction [36–38] and the extra back stress required to create the additional dislocation line length during "local" climb [39] are most attractive as both of the concepts have been shown to provide the right magnitude of the threshold stress needed in the dispersion strengthened alloys and high values of the stress exponent and activation energy [36–41]. The detachment stress, τ_d, and the extra back stress, τ_b, can be calculated using the following equations [37–39]

$$\tau_d = \frac{Gb}{\lambda}(1 - k^2)^{1/2} \tag{5}$$

and

$$\tau_b \approx 0.3\frac{Gb}{\lambda} \tag{6}$$

respectively. In the equations above, G is the shear modulus of the matrix, b is the Burgers' vector, λ is the planar spacing between reinforcement particles, and k is a relaxation parameter that takes on values between 0 for maximum attractive interaction and 1 for no attractive interaction. When $G = 49$ GPa for nickel at 1000 °C (from Equation 4), $b = 0.249$ nm [18], $\lambda = 7$ μm (determined from the microstructure of the composite), and $k = 0$ are used, τ_d and τ_b are found to be 1.74 and 0.52 MPa, respectively. However, these threshold stresses are too small to account for the observed improvement in the creep resistance of the composite, as discussed below. The threshold stress required for the improved creep resistance can be estimated using the following equation

$$\dot{\varepsilon}_c = B\left(\frac{G}{T}\right)\left(\frac{\sigma - \sigma_0}{G}\right)^{4.6}\exp\left(-\frac{Q}{RT}\right) \tag{7}$$

where $\dot{\varepsilon}_c$ represents the steady-state creep rate of the composite. Equation 7 is obtained by modifying Equation 3 with the incorporation of a threshold stress, σ_0. Substituting the steady-state creep rate ($\dot{\varepsilon}_c = 1.02 \times 10^{-7}\ s^{-1}$) of the composite with 20 vol % Y_2O_3 and the proper values for other parameters as those used in Equations 3 and 4 into Equation 7, the threshold stress is found to be 12.5 MPa which is at least one order of magnitude higher than those predicted from the detachment stress and the extra back stress for "local" climb. Thus, it is reasonable to conclude that the dislocation–particle interaction is unlikely to be responsible for the improved creep resistance of the composites.

The shear–lag modelling of nickel/yttria composites is carried out by assuming that the load transfer from the matrix to the reinforcement takes place at both the nickel/yttria interface with shear loading and the end of yttria with normal loading (Fig. 10). Furthermore, several other assumptions are made: (i) yttria particles are isolated and have a cylindrical shape; (ii) the creep of the composite is caused by matrix deformation by shearing; (iii) the matrix follows the creep law described by Equation 3; (iv) yttria is a non-creeping elastic reinforcement; and (v) there is a strong bond between yttria and nickel. With these assumptions, it can be shown that the creep rate of the composite can be expressed as follows (see the Appendix for details)

$$\dot{\varepsilon}_c = \sigma_c^{4.6}(1 - V_f)^{4.6}A \times \left[1 + 0.41V_f\frac{1}{r}\left(\frac{1}{h}\right)^{1/4.6}\left(\frac{L}{2}\right)^{5.6/4.6}\right]^{-4.6} \tag{8}$$

where σ_c is the applied stress, V_f is the volume fraction of yttria, A is a constant related to the coefficient B in Equation 3, r and L are the radius and height of yttria respectively, and $2h$ is the effective separation distance between yttria, as defined in Fig. 10. Based on the microstructure of composites with 20 and 30 vol % Y_2O_3, it is assumed that $r = 1.5$ μm and the aspect ratio of the yttria particle is one (i.e. $L = 2r$). With these assumptions, it is found that Equation 8 gives a creep rate of 6.59×10^{-6} and 2.82×10^{-6} s^{-1} for composites with 20 and 30 vol % Y_2O_3 under a stress of 20 MPa, respectively. Clearly, the predicted creep rates are one to two orders of magnitude faster than the measured creep rates (Fig. 8). It is also noted that the load transfer to isolated yttria particles leads to the same stress exponent as the matrix (see Equation 8), which is not consistent with the high stress exponent observed for the composite. Thus, the load transfer to isolated yttria particles cannot account for the improved creep resistance. A similar conclusion is also made by Dragone and Nix [31] using finite element modelling to analyse the load transfer to isolated reinforcements in A1/SiC composites and Al/Al_2O_3 composites.

The discussion above indicates that the improved creep resistance of composites with 20 and 30 vol % Y_2O_3 cannot be explained in terms of either the non-continuum mechanics concept of threshold stress or the load transfer to isolated reinforcements. It is believed that the discrepancy between the prediction and the measurement lies in the presence of a certain degree of connectivity within the yttria phase itself. Many studies [42] have shown that when the volume fraction of the second phase is larger than 20%, the second phase is expected to have interconnected clusters permeating the structure of the primary phase. For nickel/yttria composites, it has been shown that yttria can sinter to over 92% of the theoretical density at 1250 °C. Thus, some interconnected yttria clusters are expected to be present in composites with 20 and 30 vol % Y_2O_3, as confirmed by the deep-etching experiments. Using finite element modelling, Dragone and Nix [31] have shown that load transfer to an interconnected reinforcement network could give a good account of the improved creep resistance, high stress exponent and high activation energy of Al/Al_2O_3 composites. Thus, it is believed that the improved creep resistance of nickel/yttria composites with 20 and 30 vol % Y_2O_3 is caused by the presence of some interconnected yttria clusters. It is interesting to point out that if yttria particles were truly isolated, an aspect ratio of 10 for yttria particles would be required to obtain the observed improvement in the creep resistance, a result predicted based on Equation 8. This suggests that a certain degree of connectivity of the

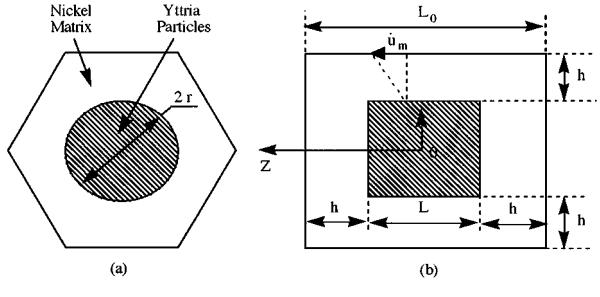

Figure 10 Schematic of the shear–lag model for nickel/yttria composites. (a) The front view and (b) the side view, showing the unit cell of a cylindrical yttria particle embedded in a hexagonal nickel matrix.

reinforcement is very effective in improving the creep resistance.

Much to our surprise, the creep resistance of composites with 40 and 50 vol % Y_2O_3 does not show a substantial improvement over the matrix. Because the microstructure examination indicates that composites with 40 and 50 vol % Y_2O_3 have a continuous Y_2O_3 network, it is expected that the creep behaviour of these composites will be dictated by the Y_2O_3 network. In order to evaluate the contribution of the Y_2O_3 network, analytical models for continuous-fibre-reinforced composites are utilized to estimate the creep rate of the nickel/yttria composite. The utilization of this approach is due to the fact that there is no rigorous analytical models available to predict the creep rate of composites with a continuous reinforcement network. Furthermore, because the yttria phase is continuous, it reasonable to assume that load can be transferred directly through the yttria network as for the case of continuous fibres in the continuous-fibre-reinforced composites. The analysis is carried out by following McDanels *et al.* [43] and McLean [44], assuming that the creep strains in the matrix and reinforcement are equal and the external load is shared by the two materials according to the rule of mixtures

$$\sigma_c = V_f\left(\frac{\dot{\varepsilon}_c}{B_f}\right)^{1/n_f} + (1 - V_f)\left(\frac{\dot{\varepsilon}_c}{B_m}\right)^{1/n_m} \quad (9)$$

where n_f and n_m are the stress exponents, B_f and B_m are temperature-dependent coefficients, subscripts f and m refer to the yttria and matrix respectively, and σ_c, $\dot{\varepsilon}_c$, and V_f have been defined in Equation 8. B_m is calculated from Equation 3 which describes the creep behaviour of the matrix, while B_f is estimated using a phenomenological equation proposed by Gaboriaud [45] for describing the creep rate of fully dense yttria, $\dot{\varepsilon}_Y$ (s^{-1}), at the temperature range between 1500 and 1800 °C

$$\dot{\varepsilon}_Y = 7.0 \times 10^6\left(\frac{G_Y}{T}\right)\left(\frac{\sigma}{G_Y}\right)^4 \exp\left(-\frac{Q}{RT}\right) \quad (10)$$

where Q is the creep activation energy and takes the value of 385.4 kJ mol^{-1}, R and T have their usual meanings, and G_Y is the shear modulus of Y_2O_3 and can be expressed as follows [46]

$$G_Y = 6.96 \times 10^{10} - 7.5 \times 10^6\ T\ (\text{Pa}) \quad (11)$$

The creep rate predicted from the McDanels' model suggests that composites with 40 or 50 vol % Y_2O_3 should have creep rates in the order of $10^{-15}\ s^{-1}$, which is much lower than those observed in the experiment (Fig. 6). The large discrepancy between the prediction and measurement may be attributed to two origins. One is the low relative density of the yttria phase obtained in the present composites. The other is that the analytical model for continuous-fibre-reinforced composites may not be suitable for composites with a continuous three-dimensional reinforcement network. It is believed that both of these sources contribute to the discrepancy. As mentioned before, the deformation of the nickel phase in composites with 40 and 50 vol % Y_2O_3 is fully constrained by the yttria network. Thus, the creep rate of the composite is primarily dependent of the creep rate of the yttria network. Pores in the yttria phase will certainly increase the intrinsic creep rate of yttria and thus increase the creep rate of the composite. Efficiencies of the load-carrying capability through a network and fibres are different even though the same strength and same volume fraction are assumed. The microstructure of composites with 40 and 50 vol % Y_2O_3 can be imagined to be composed of two interpenetrated three-dimensional networks one of which is made of the matrix and the other made of the Y_2O_3 reinforcement. Thus, the load-carrying capability of the Y_2O_3 network can be approximated by a continuous open-cell foam within which nickel is filled. For a given material and volume fraction, the stiffness and strength of an open-cell foam are lower than those of solid fibres because the deformation of fibres requires axial extension or compression, while the deformation of the foam requires bending [47]. Thus, the low relative density of the yttria phase and the low load-carrying capability of the yttria network are all contributed to the low creep resistance of the composite. Note that whether the aforementioned two sources can account for the several orders of magnitude discrepancy between the predication and experiment remains to be verified in future studies. Nevertheless, the analysis above suggests that the creep resistance of composites with high yttria volume fractions can be further improved by densifying the yttria phase and thus the composite, which can be achieved by increasing the densification temperature and pressure. A fully dense yttria phase not only improves the intrinsic creep resistance of the yttria phase, but also enhances the load-carrying capability of its three-dimensional network.

5. Concluding remarks

The feasibility of processing nickel-based composites through a powder metallurgy approach for the *in-situ* formation of a continuous three-dimensional reinforcement network or the *in-situ* formation of discrete reinforcements with certain degrees of interconnected clusters was studied using the nickel and yttria system. Despite of a large difference in the melting points of the two constituents, i.e. 2685 °C for yttria and 1455 °C for nickel, it was found that a reasonably dense, continuous Y_2O_3 network could be formed in composites with 40 and 50 vol % Y_2O_3, and discrete yttria with some degrees of interconnected clusters formed in composites with 20 and 30 vol % Y_2O_3. The creep tests of these composites indicated that the creep rate of nickel was reduced by two to three orders of magnitude with the addition of 20 to 30 vol % Y_2O_3, and it continued to decrease with increasing the volume fraction of the yttria phase.

Analyses of microstructures and creep resistances of these composites offers several general implications:

1. Densification of nickel-based composites reinforced with yttria can be carried out at temperatures

near the melting point of the matrix without the risk of the pore–grain boundary separation which led to the presence of pores in the nickel phase. This is believed to be also applicable to other metal matrix composites as long as the reinforcement is a good grain growth inhibitor. High densification temperatures will improve the density and creep resistance of the reinforcement phase and hence the creep resistance of the composite.

2. The creep resistance of metal–matrix composites could be improved over that of composites with only isolated reinforcement particles if the reinforcement particles can sinter to form interconnected clusters during the densification process.

3. At a given volume fraction, a three-dimensional reinforcement network provides less improvement in the creep resistance than fibres.

Appendix: shear–lag modelling

Equation 8 is derived based on the shear–lag analysis proposed by Kelly and Street [27]. The geometry for the shear–lag analysis of the nickel/yttria composite is shown in Fig. 10 where yttria particles are assumed to be isolated and have a cylindrical shape embedded in the nickel matrix with a hexagonal unit cell. Based on the assumed geometry, the volume fraction of the yttria phase is given by

$$V_f = \frac{3^{1/2} L \pi r^2}{6(L + 2h)(r + h)^2} \tag{A1}$$

Assuming a perfect bond at the interface, the shear rate, $\dot{\gamma}_z$, of the matrix at an average rate between a point at the interface and a point in the matrix distance h from the interface will be

$$\dot{\gamma}_z = \frac{\dot{u}_m}{h} \tag{A2}$$

where $\dot{u}_m$ is the axial velocity of the point in the matrix distance h from the interface, as shown in Fig. 10, and equals

$$\dot{u}_m = \dot{\varepsilon}_m Z \tag{A3}$$

where $\dot{\varepsilon}_m$ is the creep rate of the matrix and Z is the coordination along the yttria particle axis, as defined in Fig. 10. The shear stress at the interface, τ, can be found by assuming that the Tresca-type yield criterion holds ($\sigma_m = 2\tau$), that the matrix is incompressible ($\dot{\varepsilon}_m = \dot{\gamma}_m^{2/3}$), and that the creep of the matrix follows a power law (Equation 3) or condensed into $\dot{\varepsilon}_m = A\sigma_m^n$). Combining these assumptions with Equations 13 and 14, it can be shown that

$$\tau = \frac{1}{2}\left(\frac{2}{3}\right)^{1/n}\left(\frac{Z}{Ah}\right)^{1/n}\dot{\varepsilon}_m^{1/n} \tag{A4}$$

The stress carried by the yttria particle, σ_f, comes from the normal stress at the end of the yttria particle, σ_m, and the shear stress at the side interface, τ, and can be found with the following equation

$$\sigma_f = -\int_{L/2}^{z} \frac{2\tau}{r}\,dz + \sigma_m \tag{A5}$$

The average stress carried by the yttria particle is defined by

$$\bar{\sigma}_f = \frac{2}{L}\int_0^{L/2} \sigma_f\,dz \tag{A6}$$

and the composite stress follows the rule of mixtures

$$\sigma_c = \bar{\sigma}_f V_f + \sigma_m(1 - V_f) \tag{A7}$$

Substituting equations A4–A6 into Equation A7 the relationship between the creep rate of the matrix and the composite stress can be found. The creep rate of the composite is assumed to be proportional to the volume fraction of the matrix

$$\dot{\varepsilon}_c = (1 - V_f)\dot{\varepsilon}_m \tag{A8}$$

Thus, the final equation for the creep rate of the composite is

$$\dot{\varepsilon}_c = \sigma_c^n (1 - V_f)^n A\left[1 + V_f\left(\frac{2}{3}\right)^{1/n}\frac{1}{r} \times \left(\frac{n}{2n+1}\right)\left(\frac{1}{h}\right)^{1/n}\left(\frac{L}{2}\right)^{(1+n)/n}\right]^{-n} \tag{A9}$$

For nickel $n = 4.6$, then Equation A9 reduces to Equation 8. Note that h needed in Equation A9 can be calculated from Equation A1.

References

1. G. W. MEETHAM, "The development of the gas turbine materials" (Applied Science Publishers Ltd., New York, 1981).
2. S. OCHIAI, "Mechanical properties of the metallic composites" (Marcel Dekker, Inc., New York, 1994).
3. J. M. LARSON, W. C. REVELOS and M. L. GAMBONE, in "Intermetallic Matrix Composites II," edited by D. B. Miracle, D. L. Anton, and J. A. Graves, MRS Proceedings, Vol. 273 (Materials Research Society, Pittsburgh, PA, 1992) p. 3.
4. T. W. CHOU, A. KELLY and A. OKURA, *Composites* **16** (1985) 187.
5. L. SHAW and D. MIRACLE, *Acta Metall. Mater.* **44** (1996) 2043.
6. M. R. WISNOM, *J. Composite Mater.* **24** (1990) 707.
7. M. R. WISNOM, *J. Comp. Technol. Res.* **14** (1992) 61.
8. R. P. NIMMER, *ibid.* **12** (1990) 65.
9. R. P. NIMMER, R. J. BANKERT, E. S. RUSSELL, G. A. SMITH and P. K. WRIGHT, *ibid.* **13** (1991) 3.
10. R. W. EVANS and B. WILSHIRE, "Introduction to creep" (The Institute of Materials, Swansea, 1993).
11. F. THUMMLER and R. OBERACKER, "An introduction to powder metallurgy" (The Institute of Materials, London, 1993).
12. C. E. CURTIS, *J. Amer. Ceram. Soc.* **40** (1957) 274.
13. M. DESMAISON-BRUT and J. MONTINTIN, *ibid.* **78** (1995) 716.
14. E. N. DA C. ANDRADE, *Proc. R. Soc. Lond., A.* **84** (1911) 1.

15. N. F. MOTT, *Phil. Mag.* **44** (1953) 742.
16. C. K. L. DAVIES, P. W. DAVIES and B. WILSHIRE, *ibid.* **12** (1965) 827.
17. A. K. MUKHERJEE, J. E. BIRD and J. E. DORN, *Trans. ASM* **62** (1969) 155.
18. M. F. ASHBY, *Acta Metall.* **20** (1972) 887.
19. W. BETTERIDGE, "Nickel and its alloys" (Ellis Horwood Limited, UK 1984).
20. T. G. NIEH, K. XIA and T. G. LANGDON, *J. Eng. Mater. Technol.* **110** (1988) 77.
21. V. C. NARDONE and J. R. STRIFE, *Metall. Trans.* **18A** (1987) 109.
22. K.-T. PARK, E. J. LAVERNIA and F. A. MOHAMED, *Acta Metall.* **38** (1990) 2149.
23. G. GONZALEZ-DONCEL and O. D. SHERBY, *ibid.* **41** (1993) 2797.
24. R. S. MISHRA and A. B. PANDEY, *Metall. Trans.* **21A** (1990) 2089.
25. A. B. PANDEY, R. S. MISHRA and Y. R. MAHAJAN, *Acta Metall. Mater.* **40** (1992) 2045.
26. A. KELLY and K. N. STREET, *Proc. R. Soc. Lond., A.* **328** (1972) 267.
27. A. KELLY and K. N. STREET, *ibid.* **328** (1972) 283.
28. T. MORIMOTO, T. YAMAOKA, H. LILHOLT and M. TAYA, *Trans. ASME* **110** (1988) 70.
29. V. C. NARDONE and K. M. PREWO, *Scripta Metall.* **20** (1986) 43.
30. T. L. DRAGONE and W. D. NIX, *Acta Metall. Mater.* **38** (1990) 1941.
31. T. L. DRAGONE and W. D. NIX, *ibid.* **40** (1992) 2781.
32. R. J. ARSENAULT and R. M. FISHER, *Scripta Metall.* **17** (1983) 67.
33. M. VOGELSANG, R. J. ARSENAULT and R. M. FISHER, *Metall. Trans.* **17A** (1986) 379.
34. R. J. ARSENAULT and M. TAYA, *Acta Metall.* **35** (1987) 651.
35. R. J. ARSENAULT and N. SHI, *Mater. Sci. Eng.* **81** (1986) 175.
36. V. C. NARDONE, D. E. MATEJCZYK and J. K. TIEN, *Acta Metall.* **32** (1984) 1509.
37. E. ARZT and D. S. WILKINSON, *ibid.* **34** (1986) 1893.
38. E. ARZT and J. ROSLER, *ibid.* **36** (1988) 1053.
39. E. ARZT and M. F. ASHBY, *Scripta Metall.* **16** (1982) 1285.
40. J. D. WHITTENBERGER, *Metall. Trans.* **15A** (1984) 1753.
41. T. E. HOWSON, D. A. MERVYN and J. K. TIEN, *ibid.* **11A** (1980) 1609.
42. R. M. GERMAN, "Particle packing characteristics" (Metal Powder Industries Federation, New Jersey, 1989).
43. D. L. MCDANELS, R. A. SIGNORELLI and J. W. WEETON, NASA Tech. Note, NASA-TN-D-4173, 1967.
44. M. MCLEAN, "Directionally solidified materials for high temperature service" (The Metals Society, London, 1983).
45. P. R. J. GABORIAUD, *Phil. Mag.* **44A** (1981) 561.
46. D. R. WILDER and M. O. MARLOWE, *J. Amer. Ceram. Soc.* **48** (1965) 227.
47. L. J. GIBSON and M. F. ASHBY, "Cellular solids: structure and properties" (Pergamon Press, UK 1988).

Received 28 January
and accepted 16 June 1998